Lopez Del Amo, V.; Palomino-Schätzlein, M.; Seco-Cervera, M.; Garcia-Gimenez, JL.; Pallardó-Calatayud, FV.; Pineda-Lucena, A.; Galindo-Orozco, MI. (2017). A Drosophila model of GDAP1 function reveals the involvement of insulin signalling in the mitochondria-dependent neuromuscular degeneration. Biochimica et Biophysica Acta (BBA) - Molecular Basis of Disease. 1863(3):801-809. https://doi.org/10.1016/j.bbadis.2017.01.003

A *Drosophila* model of *GDAP1* function reveals the involvement of insulin signalling in the mitochondria-dependent neuromuscular degeneration.

Víctor López del Amo[1,2,$], Martina Palomino-Schätzlein[1,$], Marta Seco-Cervera[2,3], José Luis García-Giménez[2,3], Federico Vicente Pallardó[2,3], Antonio Pineda-Lucena[1,4] and Máximo Ibo Galindo[1,5,6,*]

[1] Centro de Investigación Príncipe Felipe, 46012 Valencia. Spain

[2] Center for Biomedical Network Research on Rare Diseases (CIBERER), 46012 Valencia. Spain.

[3] Department of Physiology, School of Medicine and Dentistry, Universitat de València, INCLIVA Biomedical Research Institute, 46010 Valencia. Spain.

[4] Drug Discovery Unit, Instituto de Investigación Sanitaria La Fe, 46026 Valencia. Spain.

[5] IDM-Institute of Molecular Recognition, Universidad Politécnica de Valencia, 46022 Valencia. Spain.

[6] UPV-CIPF Joint Unit Disease Mechanisms and Nanomedicine

* To whom correspondence should be addressed at: igalindo@cipf.es

[$] These authors contributed equally.

ABSTRACT

Charcot-Marie-Tooth disease is a rare peripheral neuropathy for which there is no specific treatment. Some forms of Charcot-Marie-Tooth are due to mutations in the *GDAP1* gene. A striking feature of mutations in GDAP1 is that they have a variable clinical manifestation, according to disease onset and progression, histology and mode of inheritance. Studies in cellular and animal models have revealed a role of *GDAP1* in mitochondrial morphology and distribution, calcium homeostasis and oxidative stress. To get a better understanding of the disease mechanism we have generated models of over-expression and RNA interference of the *Drosophila Gdap1* gene. In order to get an overview about the changes that *Gdap1* mutations cause in our disease model, we have combined a comprehensive determination of the metabolic profile in the flies by nuclear magnetic resonance spectroscopy with gene expression analyses and biophysical tests. Our results revealed that both up- and down-regulation of *Gdap1* results in an early systemic inactivation of the insulin pathway before the onset of neuromuscular degeneration, followed by an accumulation of carbohydrates and an increase in the β-oxidation of lipids.

Our findings are in line with emerging reports of energy metabolism impairments linked to different types of neural pathologies caused by defective mitochondrial function, which is not surprising given the central role of mitochondria in the control of energy metabolism. The relationship of mitochondrial dynamics with metabolism during neurodegeneration opens new avenues to understand the cause of the disease, and for the discovery of new biomarkers and treatments.

KEYWORDS: GDAP1, Charcot-Marie-Tooth, mitochondria, insulin.

1. INTRODUCTION

The Charcot-Marie-Tooth (CMT) disease (ICD-10: G60.0) refers to those forms of inherited peripheral neuropathies in which both the motor and sensory functions are affected [1]. Despite the fact that there are several types of CMT, collectively they affect one in 2.500 people, so it is considered a rare disease. In CMT, neuromuscular degeneration is dependent on the length of the axon, so it affects primarily the long nerves of the limbs, starting with the lower limbs. The loss of muscle mass results in deformities in foot and hand (*pes cavus*, hammertoes, claw hands) and in an "inverted champagne bottle" appearance of the distal leg. There are two main clinical forms of CMT that are classified according to motor nerve conduction velocity in the upper limb nerves, Demyelinating CMT (CMT1) is characterized by a decreased motor nerve conduction velocity (<38 m/s) and dysmyelination traits in sural nerve biopsies; while axonal CMT (CMT2) patients present normal or slightly reduced motor nerve conduction velocity (>42 m/s) and no dysmyelination phenotypes despite a reduction in the number of axons [1, 2]. CMT is also a genetically heterogeneous disease, with over 50 genes harbouring CMT-causative mutations and all major modes of inheritance: autosomal recessive, autosomal dominant and X-linked.

Two of the most common causative genes for axonal CMT2, *MFN2* and *GDAP1*, are involved in mitochondrial dynamics. Many studies have described mitochondrial dynamics as an underlying cause for neurodegenerative diseases [3]. The balance of mitochondrial fission and fusion contributes primarily to mitochondrial morphology, but it is also crucial for the correct localization of these organelles within the cell and for several processes such as oxidative phosporylation, autophagy, calcium homeostasis, cell differentiation and cell death [4]. Mutations in the *GDAP1* gene have been found to be a cause of at least 4 different subtypes of Charcot-Marie-Tooth (A, 2K, 4A and autosomal recessive CMT with hoarseness) and is also a candidate causative gene for CMT2H [5, 6]; and the GDAP1 protein, located in the

mitochondrial outer membrane, has been described as a fission factor regulating the mitochondrial network [7, 8], peroxisome morphology [9] and store-operated calcium entry dependent on ER-mitochondria contacts [10]. Two murine models of *Gdap1* knock-out show peripheral neuropathy and alterations in oxidative stress and store-operated calcium entry [11, 12]. A *Drosophila* model of GDAP1 reproduces the hallmarks of neuromuscular degeneration, and has revealed mitochondrial morphology and distribution alterations as early features, and oxidative stress alterations as a late-onset consequence of altered levels of the protein [13].

Mitochondrial dynamics is intimately associated with neurodegeneration [14], but mitochondria are also central organelles in the control of metabolism and mitochondrial dynamics has a leading role in metabolic diseases such as diabetes and obesity [15]. Therefore, it is not surprising that there is mounting evidence of concomitant metabolic and neural dysfunctions. For example, an increase in mitochondrial fission and disturbance in tricarboxylic acid (TCA) cycle metabolites associated with Alzheimer disease, or an alteration in glucose and coenzyme Q homeostasis triggered by the ablation of CMT-related Mfn2 [16, 17].

We decided to use *Drosophila* to investigate metabolic changes caused by altered *Gdap1* expression with the aims to have a better understanding of the CMT pathophysiology and to reveal metabolic alterations that could lead to the discovery of biomarkers of diagnostic and prognostic value, which is a priority in CMT translational research [18]. The global metabolic profile analysis of our *Drosophila* disease model by nuclear magnetic resonance (NMR) spectroscopy in combination with the quantification by PCR and Western blotting of related pathway genes and proteins reveals extensive alterations in the energy metabolism and a dys-regulation of the insulin signaling pathway. These results are discussed in the context of what is known about the clinical genotype-phenotype correlation.

RESULTS

1.1. *Gdap1* levels influence fitness and age-related neuromuscular competence

To identify systemic alterations associated with the pathophysiology of *GDAP1*-related CMT, *Drosophila Gdap1* levels were altered in the whole animal using the *UAS/Gal4* technique [19]. A ubiquitous driver, *Ac5C-Gal4*, was used to express a *Gdap1* cDNA (kick-up, KU flies) and an RNAi directed against the gene (knock-down, KD flies). These constructs have been previously validated for up- and down-regulation of *Gdap1* expression [13]. Both KU and KD genotypes compromise the viability of the animals (Fig. 1A), since they reduce the maximum lifespan, 90 days, by 40 and 20 days, respectively. In addition, both genotypes also have a reduced neuromuscular competence measured in a negative geotaxis assay (Fig. 1B and Video S1); and they suffer a progressive deterioration in the ability to climb the vial wall, although this defect was more pronounced in the KD flies. Therefore, the more reduced viability of KU is not due to a lower neuromuscular competence, and other factors must contribute to this. Finally, we calculated the average body weight per individual as an indication of the overall metabolic alterations, and found a significant reduction in older KU flies (Fig. 1C).

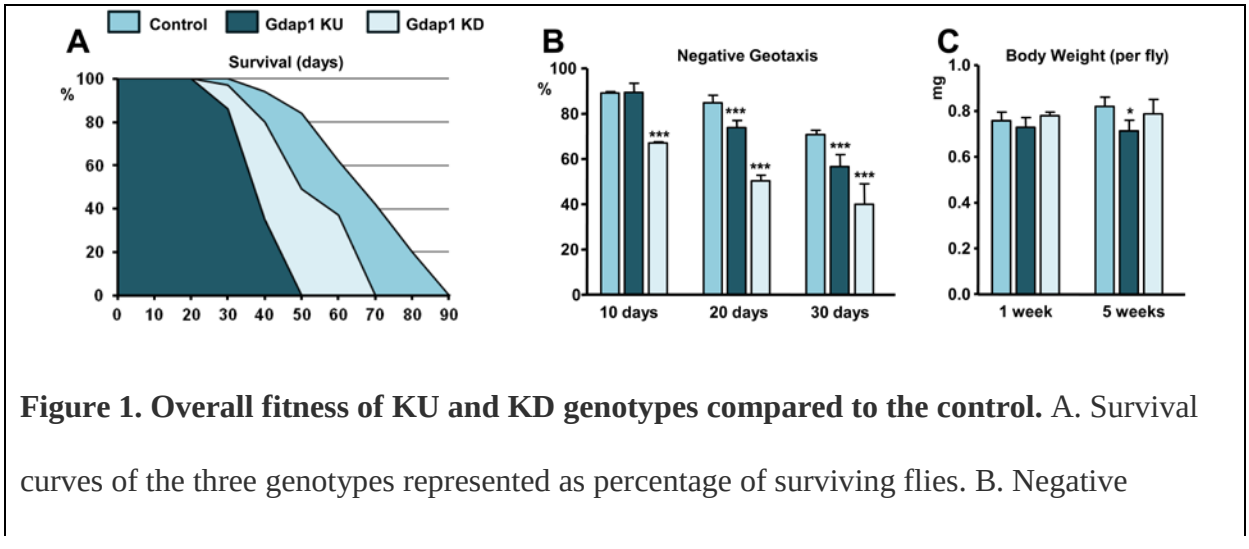

Figure 1. Overall fitness of KU and KD genotypes compared to the control. A. Survival curves of the three genotypes represented as percentage of surviving flies. B. Negative

geotaxis assay at 10, 20 and 30 days of age. C. Average body weight at 1 and 5 weeks. In bar diagrams data are represented as mean ±SEM. *P<0.05, ***P<0.001.

1.2. Impact of *Gdap1* expression on the general metabolic profile

As mitochondrial defects can have an impact in several metabolic pathways, we decided to analyze the alterations in the metabolome of the KU and KD genotypes by NMR spectroscopy. We performed metabolomic analyses at two ages, 1 week and 5 weeks of adult life (henceforth, young and old flies), to detect early alterations that may be related to the cause of the neuromuscular degeneration, and later ones, that could reflect the progression of the phenotype. We characterized the metabolic profile of polar and non-polar fly extracts by high resolution NMR, and of intact fly tissue by High Resolution Magic Angle Spinning (HR-MAS) (Figure 2).

A detailed analysis of the spectral peaks in all three genotypes is shown in Tables S1 to S5. After metabolite assignment, the relative abundance of each metabolite in all three genotypes was determined to evalute the differences between each set. This evaluation was followed by a multivariate statistical analysis to identify the most significant changes in the metabolic profiles. Orthogonal projection on latent structure-discriminant analysis (OPLS-DA) was performed to build the models based on the metabolic differences of Gdap1 KU and KD genotypes compared to control flies at both time periods. In the case of young flies, it was not possible to obtain a reliable model, separating KU or KD flies from the control ones. However, good quality models were obtained for old flies, with R2 values close to 1, and Q2 values>0.5. (Fig. 3A, B). This is in agreement with our previous work [13], where no significant physiological differences were detected in young flies.

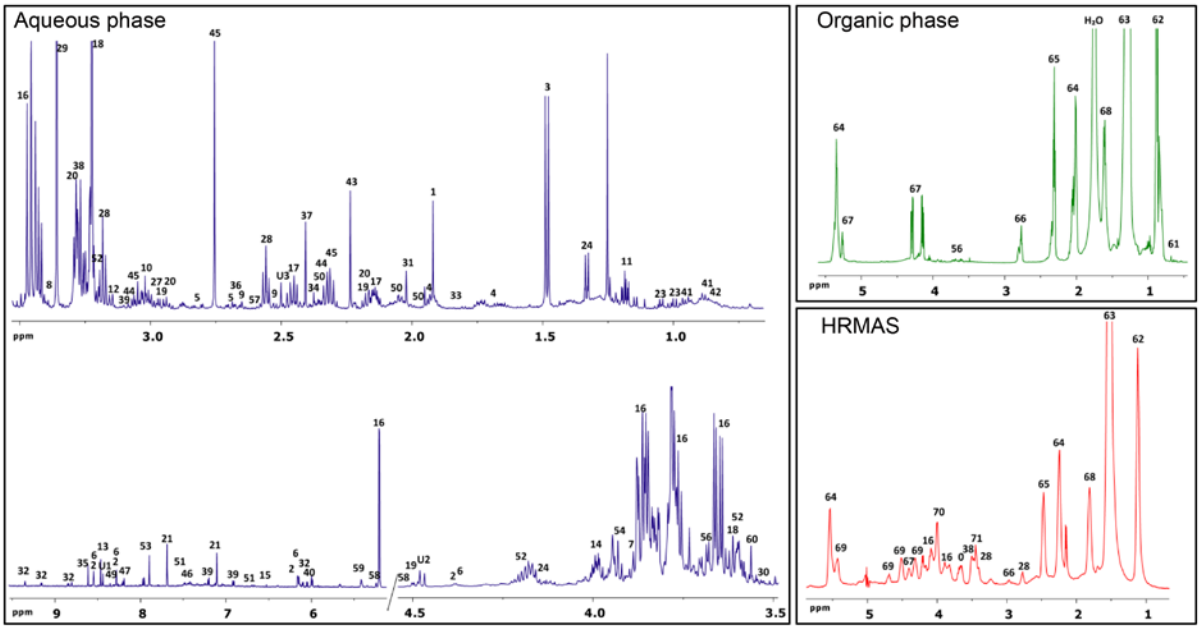

Figure 2. Representative NMR spectra of fly extracts with peak assignation. The spectra for the aqueous phase (blue), the organic phase (green) and HR-MAS (red) of a control sample are shown. The labels above the peaks correspond to the same identifiers indicated in Tables S1 to S5. The highest diversity of metabolites was detected in the aqueous phase, which included sugars, amino acids, organic acids, nucleotides and other key metabolites of the energetic and phospholipid metabolism. The spectrum of the organic phase presented broader signals and contained mainly lipids. NMR spectroscopy only allows the identification of the functional groups of different lipid types due to the high degree of overlapping. In addition to conventional NMR spectroscopy, we obtained HR-MAS spectra of intact tissue, containing both polar and nonpolar metabolites. Although the resolution of these spectra is much lower, this technique allows the analysis of the whole living fly without any tissue processing and allows a better detection of more mobile molecules, which could provide interesting additional information concerning the lipid profile.

In these 5-week old flies the S-plots showed the most relevant metabolites involved in the discrimination (Fig. 3A, B). The most relevant changes belonged to carbohydrates, some of which were elevated in KU (myo-inositol), KD (glucose, glycogen, trehalose) or both (fructose); and in amino acids, whose levels were generally reduced in both genotypes, with the exception of alanine (elevated in KU) and arginine (elevated in KD). Both models showed an increase in glycerophosphocholine (GPC), a metabolite that accumulates in cerebrospinal fluid of Alzheimer patients as a result of membrane phospholipid degradation during neurodegeneration [20].

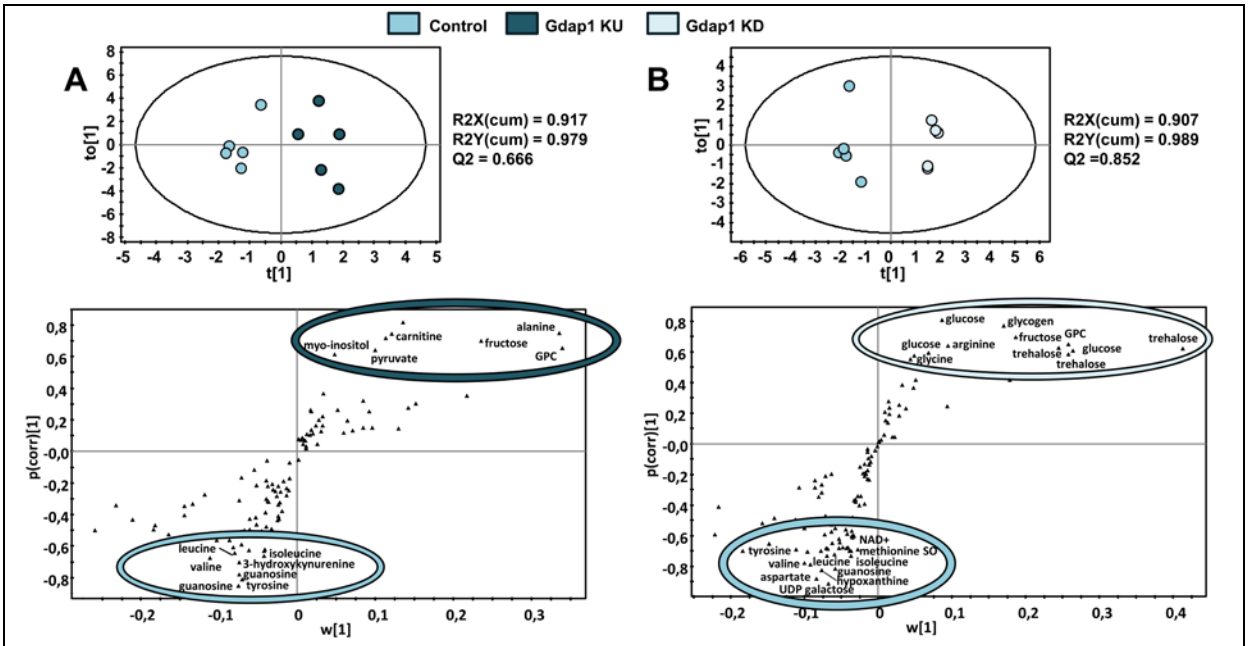

Figure 3. Metabolic profile of KU and KD genotypes compared to the control. A. OPLS-DA score plot comparing KU flies to control flies at five weeks of age and corresponding S plot, color coded circles enclose the metabolites that are most relevant for the separation. B. The same analysis was performed to compare KD flies to control flies.

It is worth mentioning that although both genotypes showed the same trends in some types of metabolites, a discriminant model for KU compared to KD was also built (see Supplementary

Material Fig S1), which means that although similar metabolic routes may be affected in both cases (see below), the two genotypes have two distinct metabolic profiles.

In summary, the most significant metabolic changes in KU and KD genotypes point to alterations in the levels of free amino acids and, most remarkably, in the carbohydrate metabolism. These metabolites provided a starting point to investigate additional metabolites exhibiting statistical significance that could provide clues to the biological function of Gdap1. In addition, we have studied the expression levels of enzymes that regulate the pathways involved in metabolite abundance. Since young flies do not have many relevant changes, these analyses only focused on old flies.

1.3. The amino acid profile is consistent with a protein anabolism/catabolism imbalance

In Fig. 4A, a more detailed overview of the differences in amino acids in old flies is shown. There is a consistent reduction in the amounts of β-alanine, aspartate, isoleucine, leucine, valine and tyrosine, and an increase of alanine in KU and of arginine in KD. Several lines of evidence indicate that these results are associated with a catabolic process. This set includes the three branched-chain amino acids, which promote protein synthesis in the muscle [21]. Our profile is very similar to the amino acid abundance in plasma of amyotrophic lateral sclerosis patients [22]. In this regard,, patients had reduced levels of aspartate, isoleucine, leucine, valine and tyrosine compared to healthy controls. In addition, higher levels of alanine were linked to a clinical terminal state and higher levels of arginine to faster progression of the disease. A reduction in the muscular metabolite β-alanine has been associated with muscle degeneration in *Drosophila* [23].

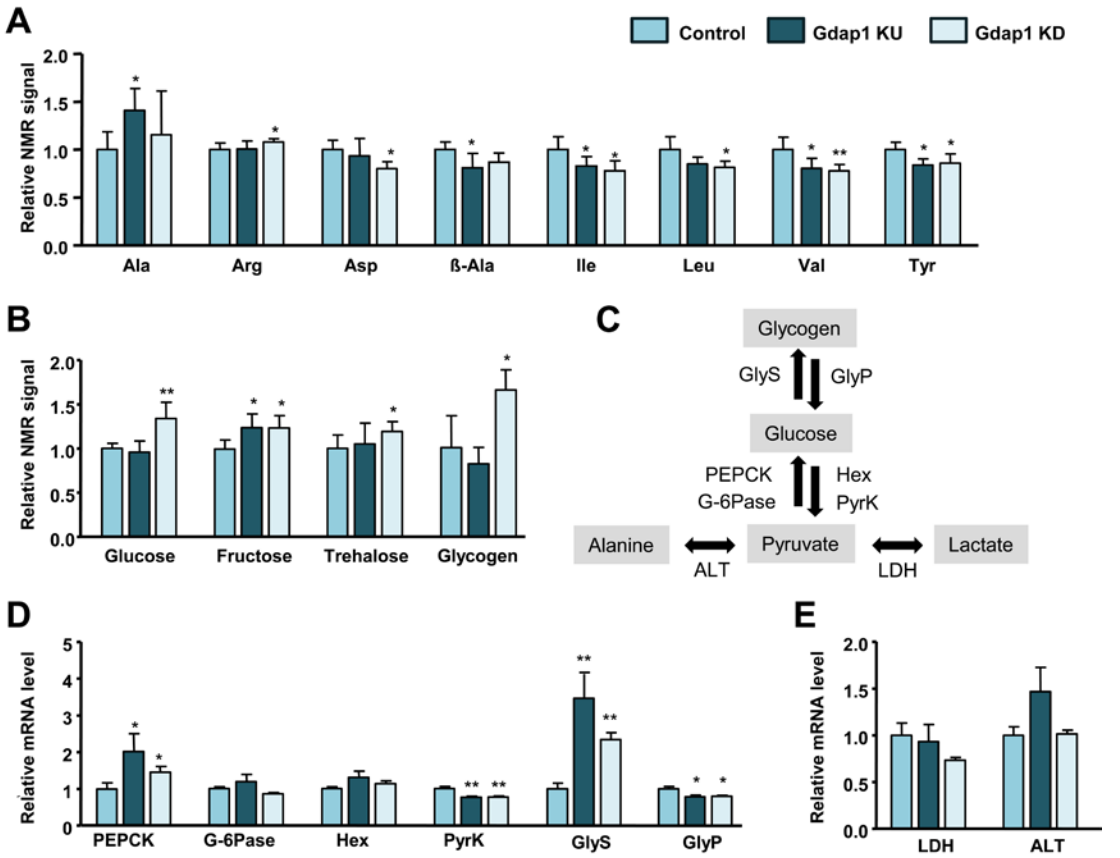

Figure 4. Alterations in amino acid and carbohydrate homeostasis in 5-week old flies. A. Relative NMR signals of amino acids with significant changes. B. Relative NMR signals of carbohydrates with significant changes. C. Schematic representation of the metabolic pathways of carbohydrates and extra-mitochondrial pyruvate, with indication of the key enzymes quantitated in our work. D. Relative mRNA level of carbohydrate metabolism enzymes. E. Relative mRNA levels of pyruvate metabolism enzymes. In bar diagrams data are represented as mean ±SEM. *P<0.05, **P<0.01.

1.4. Alterations in *Gdap1* levels translate into accumulation of carbohydrates

A general trend in the metabolic profile of old KU and KD flies is an average increase in carbohydrates (Fig. 4B). In KD flies we found a significant increase in glucose, fructose, trehalose and glycogen, and an increase of fructose levels in KU flies. In agreement with this

finding, both genotypes had increased transcript levels of the gluconeogenesis regulator phosphoenolpyruvate carboxykinase (PEPCK) and the glycogen synthase (GlyS); and reduced levels of the glycolytic enzyme pyruvate kinase (PyrK) and the glycogenolytic enzyme glycogen phosphorylase (GlyP) (Fig. 4C, D). In summary, altering *Gdap1* levels causes an accumulation of different carbohydrates and a transcriptional response in favor of anabolism and against catabolism of carbohydrates.

Despite this accumulation of carbohydrates, pyruvate levels were slightly increased rather than reduced (see below), so we tested two other branching pathways for pyruvate metabolism towards alanine and lactate (Fig 4C). Although alanine was elevated, more significantly in KU, no significant alterations were detected in the expression of alanine transaminase (ALT) and lactate dehydrogenase (LDH) (Fig 4E).

1.5. Modified Gdap1 levels trigger a switch-over in the energy use

Pyruvate is the bridge between glycolysis and the TCA cycle, and its levels are controlled by the pyruvate dehydrogenase complex (PDC), which regulates the entry of glycolytic products to the TCA cycle, converting pyruvate to acetyl-CoA (Fig. 5A). The activity of PDC is tightly controlled by both, the inhibitor pyruvate dehydrogenase kinase (PDK) and the activator pyruvate dehydrogenase phosphatase (PDP)[24]. Both enzymes are regulated at the transcriptional level, and in our study we found that KD flies had reduced levels of PDP and both KU and KD had elevated levels of the inhibitor PDK (Fig. 5B). In addition to its transcriptional control, PDK acts as a sensor of physiological information to regulate PDC: a high ratio NADH/NAD^+ and high levels of mitochondrial ATP activate PDK, which in turn inhibits the activity of PDC. Regarding these two parameters, both genotypes showed a high ratio NADH/NAD^+ and also high levels of mitochondrial ATP (Fig. 5B). These results

suggest that PDC must be down-regulated and this would explain that there is no reduction in pyruvate levels despite the glycolysis was impaired. However, the abundances of some of the most important TCA cycle metabolites were similar to the control (Fig. 5C), suggesting compensatory changes in the production of acetyl-CoA to maintain the homeostasis of TCA cycle. If glycolisis is impaired, there must be an alternative anaplerotic pathway to feed the TCA cycle, such as lipid oxidation. This could also explain the decrease in $NADH/NAD^+$ ratio and ATP, since lipolysis is more energetic than oxidative phosphorylation via glycolysis and TCA cycle. In fact, PDC is the main regulator of the choice of carbohydrates or lipids as metabolic fuel [25].

To detect changes in lipid metabolism, we explored HR-MAS spectra, since they provide predominantly signals from dynamic lipids, reducing the interference of the more static membrane lipids (Fig. 5D). We observed a reduction in the amount of total lipids in KU and KD flies. In addition, we carried out a more detailed analysis of specific lipid types; unsaturated lipids, esterified lipids, triacylglycerols and phospholipids, and we observed reduction in most of them, especially in the KD genotype. As a further proof of the imbalance in lipid metabolism, we quantitated the expression of two genes that have been shown to reflect transcriptional control of this process in *Drosophila* (Fig 5A): transcript levels of *CG6178*, related with lipogenesis [26], were strongly reduced; while transcripts of the glucagon analog adipokinetic hormone receptor (*AKHR*), which participates in lipid mobilization [27] where significantly increased in KD.

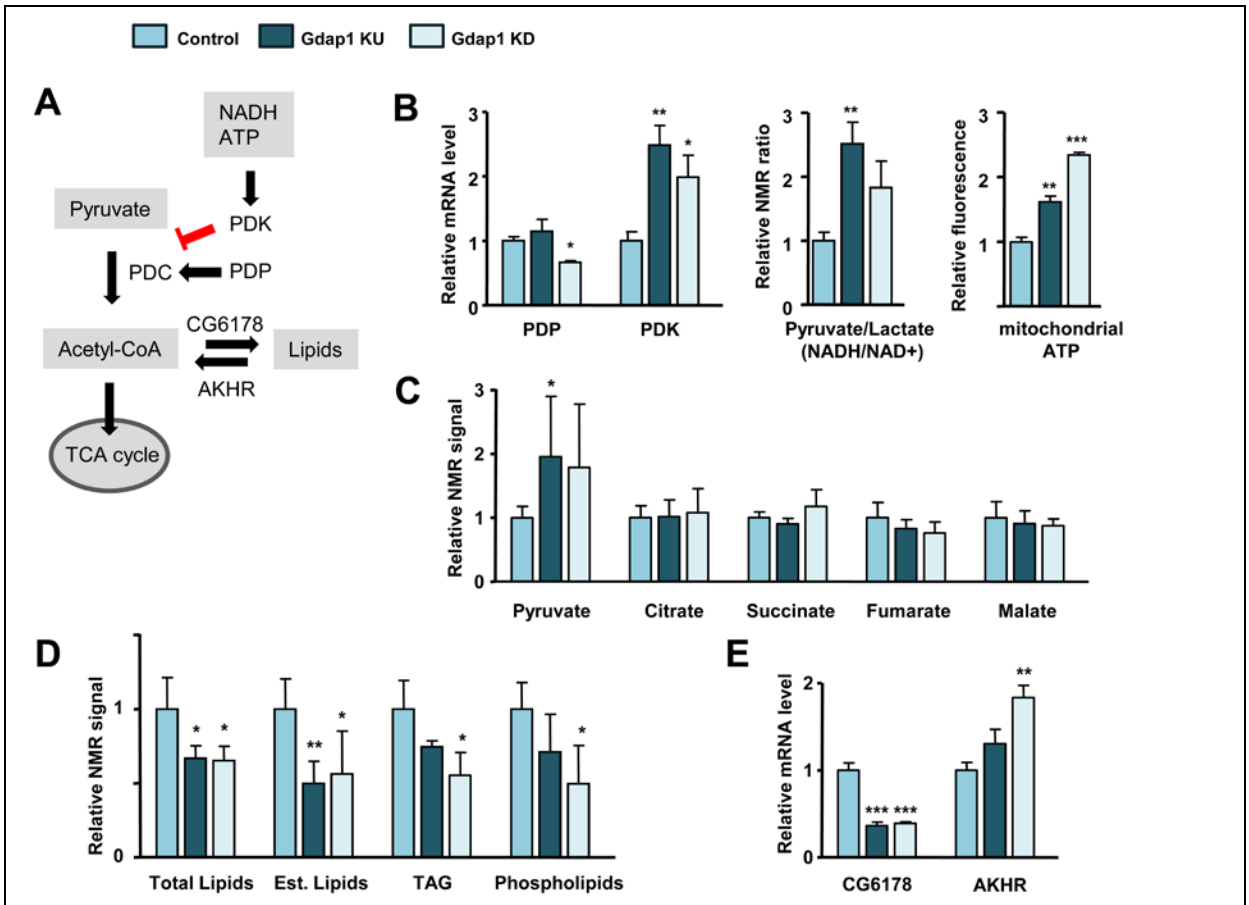

Figure 5. Anaplerotic shift to β-oxidation of lipids in 5-week old flies. A. Schematic representation of the regulation of Acetyl-CoA synthesis from mitochondrial pyruvate and β-oxidation of lipids, with indication of the enzymes and metabolites analysed. B. Estimation of the mRNA levels of PDP and PDK, relative ratios of pyruvate/lactate and relative mitochondrial ATP abundance as an indication of PDC activation. C. Relative NMR signal of pyruvate and key TCA cycle metabolites. D. Relative NMR signals of lipids with significant changes. E. Relative mRNA abundance of lipid metabolism enzymes. In bar diagrams data are represented as mean ±SEM. *P<0.05, **P<0.01, ***P<0.001.

1.6. A systemic early deficit of insulin signaling precedes the defects in carbohydrate and lipid homeostasis

Both the KU and the KD models showed a shift in metabolic fuel selection, which is most accused in the latter. Similar alterations are usually due to a down-regulation of the insulin pathway. When the insulin pathway is activated, Akt is phosphorylated, and it turn it phosphorylates FOXO, which is then retained in the cytosol for its degradation. When FOXO is not phosphorylated, it translocates to the nucleus to function as a transcriptional regulator. One of the FOXO targets is the PDC negative regulator PDK, so one of the main roles of FOXO activation is to favor fatty acid oxidation [28], which is consistent with our observations. The contact of mitochondria and endoplasmic reticulum (ER) through the mitochondria-associated membranes (MAMs) is an important modulator of insulin signaling, wherefore an excess or reduction of this contact causes insulin-signaling defects [29, 30]. Tethering of mitochondria to the ER is precisely one of the functions of GDAP1, and GDAP1 over-expression increases the contact of these organelles, while RNAi has the opposite effect [10]. Our hypothesis is that up- and down-regulation of *Gdap1* alters mitochondria-ER contacts and as a consequence there is a deficiency in insulin signaling. To test this hypothesis, we investigated whether mitochondria-ER contacts and the insulin pathway were altered in our fly models. Most importantly, we performed these experiments in young flies, before major metabolic alterations are detectable.

Our previous work revealed alterations in mitochondrial morphology and localization in 1-week old models of *Gdap1* KU and KD in the fly retina neurons [13]. The retina is a nervous tissue where quantitative ultrastructural studies can be performed. We re-analyzed these electron micrographs to calculate the number of mitochondria in contact with the ER in proportion with the total number of mitochondria (Fig. 6A, B). As it could be expected, this analysis revealed that, when compared with control flies, KU retinas had more contacts than KD ones.

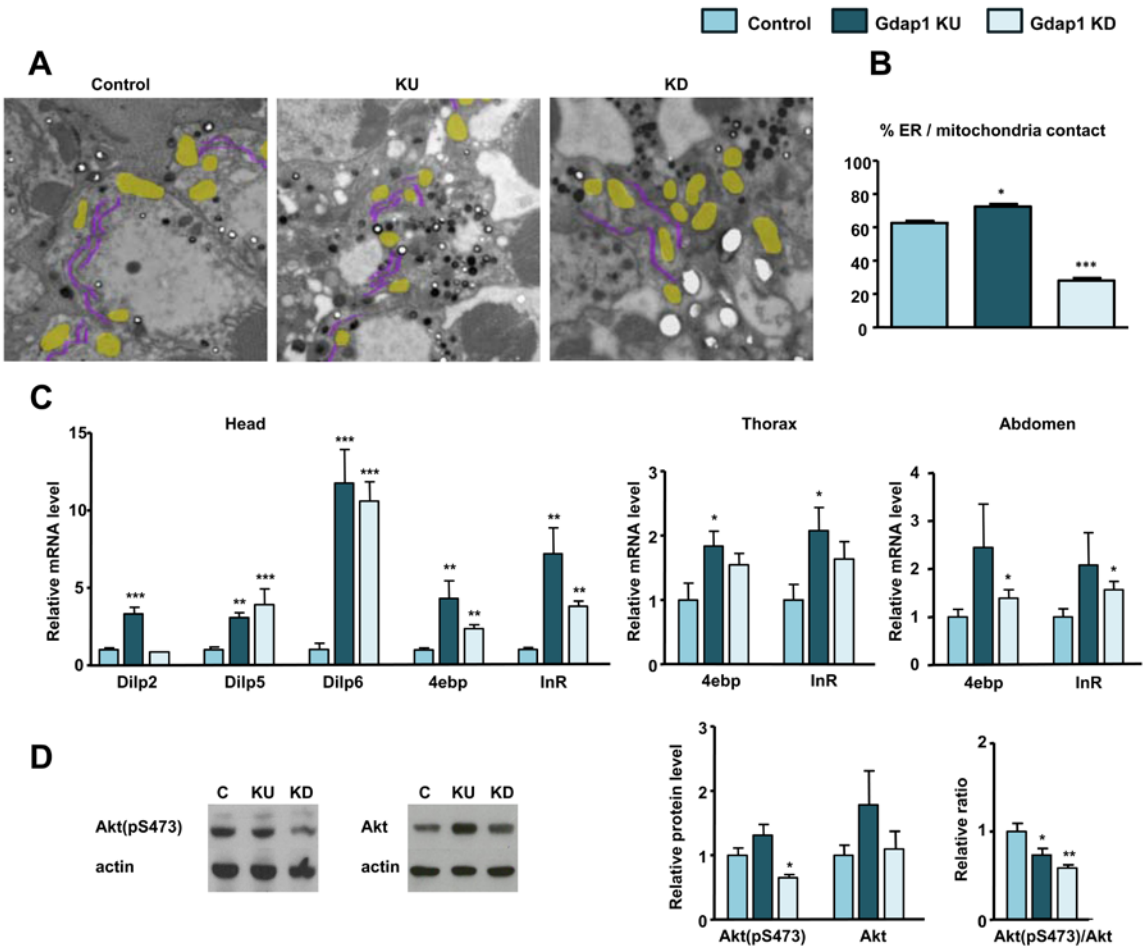

Figure 6. Alterations in mitochondria-ER contacts and insulin signaling in 1-week old flies. A. Details of representative micrographs of retinas of the three genotypes with mitochondria highlighted in yellow and ER in magenta. B. Quantitation of the percentage of mitochondria in contact with the ER. C. Relative mRNA levels of Dilps, 4EBP and InR in separated head, thorax and abdomen samples. D. Representative Western blots for phosphorylated-Akt (Ser473) and total Akt in the three genotypes, and quantitation of the protein abundance and protein ratio in five replicates. In bar diagrams data are represented as mean ±SEM. *P<0.05, **P<0.01, ***P<0.001.

In order to have a general view of the activation of the insulin-signaling pathway, we measured the expression levels of the *Drosophila* insulin-like peptides (Dilps, Fig 6C), in

head extracts, since these peptides are produced in neuroendocrine cells located in the head [31]. On average, expression of *Dilp3*, *Dilp5* and *Dilp6* was up-regulated, most dramatically for *Dilp6*. High mRNA levels of these genes could be a response to counterbalance for the increase in glycaemia in both genotypes. In addition, we checked the expression of two insulin suppression markers, *4ebp* and the insulin receptor (*InR*). These genes are transcriptional targets of FOXO, and in conditions of insulin pathway deficiency their expression is up-regulated [32]. The expression of *4ebp* and *InR* was strongly elevated in both genotypes in the head, the source of the signal, but also in thorax and abdomen, indicating a systemic deficiency in insulin signaling (Fig. 6C).

The range of immunological tools in *Drosophila* is narrower than in mammalian models, but at least it is possible to test the phosporylation state of Akt as a confirmation of the down-regulation of the pathway. We estimated the abundance of total Akt and phospho-Akt (Ser473) in protein extracts from fly heads. We found a significant reduction in the phospho-Akt to total Akt ratio in both genotypes, although this could be due to different reasons (Fig 6D). In the KU flies, phospho-Akt levels are not different from the control, but total Akt is more abundant. In contrast, in KD flies total Akt is normal but it is less phosphorylated. These features, lower proportion of p-AKT, high *Dilp* expression, insulin suppression markers (4ebp and InR), and high glycaemia in the longer term, are akin to insulin resistance.

2. DISCUSSION

2.1. Metabolic and mitochondrial alterations in flies with altered *Gdap1* levels

In this work we have performed the first NMR metabolomic analysis focused on a *Drosophila* disease model, and our results indicate that this can be a useful tool in pathophysiology research and biomarker discovery. In addition to metabolic changes that could be expected, such as an amino acid profile consistent with muscular degeneration, our results show that *Gdap1* expression levels are important in the regulation of mitochondria-ER contacts and the insulin pathway. Perturbations of these events are evident early in the life of the *Gdap1* KU and KD flies, and precede other metabolic changes. In older flies, there are significant changes in metabolites related to neuronal and muscular degeneration, and a shift in the energy metabolism that favours lipid use as an energy source in detriment of carbohydrates. Our results suggest a chain of events linking mitochondrial dynamics to insulin signaling to energy metabolism, that can contribute to the disease mechanisms related to mutations in *GDAP1* and other genes involved in mitochondrial dynamics and neurodegeneration.

The fact that we observe similar alterations in energy metabolism may seem counter-intuitive, but a detailed analysis of our data and the clinical picture in mitochondrial CMT reveals that these observations are consistent and can be important to understand some of the underlying disease mechanisms. First, the KU and KD models are not identical, although they showed similar alterations in insulin signalling and metabolic profile. In fact, we could obtain a model to separate them at five weeks of age, which shows that they have distinct metabolic profiles in spite of the similarities that we have highlighted. Most important, the fact that tilting the balance of mitochondrial fusion and fission in any direction can produce a similar phenotype is evident from the genetics of mitochondrial CMT patients. In principle, GDAP1 and MFN2

have opposite effect in mitochondrial dynamics, since they promote mitochondrial fission and fusion respectively, although this may be an oversimplification.

Several experiments mainly in cell culture have demonstrated that expression of wild type GDAP1 promotes fragmentation but does not prevent fusion, and that dominant and recessive mutations have different effects on this function of the protein [7, 10, 33, 34]. Truncating and missense recessive mutations produce a loss of function and therefore have reduced fragmentation activity, in contrast dominant mutations maintain this activity and instead prevent fusion. Therefore, dominant and recessive alleles of *GDAP1* can cause a similar phenotype by affecting mitochondrial dynamics by opposite mechanisms.

In summary, an imbalance in mitochondrial fusion/fission dynamics in either direction can result in peripheral neuropathy. If the mitochondrial network is too fragmented or too aggregated several mitochondrial-related processes are impaired, such as sub-cellular localisation, mitochondrial respiration or mitochondria-ER contact-dependent calcium homeostasis. Our results show that correct insulin signalling is also dependent on a properly balanced mitochondrial dynamics and this could be one of the disease mechanisms contributing to mitochondrial CMT neuropathy.

2.2. Emerging links of mitochondrial dynamics, metabolism and neurodegeneration

There is mounting evidence of metabolic alterations in neurodegenerative diseases, especially those that involve deregulation of mitochondrial function, structure and localization. A metabolic shift similar to our *Gdap1* model has been described in a mouse model of ALS, another motor neuron disease, involving reduced glycolysis, enhanced lipolysis and up-regulation of PDK [35]. Diabetes has also been found to be related to neurodegenerative

diseases such as Alzheimer's disease [36] and Friedreich's ataxia[37]. Insulin signalling and PDK activity seem to be central to this link [38].

This could very well be the case in CMT neuropathy, since several CMT-causing mutations and CMT-related genes have a clear metabolic implication. Most strikingly, the other main mitochondrial dynamics gene, MFN2, has clear functional links with energy metabolism. Studies in mouse *Mfn2* have revealed that its effects in mitochondrial dynamics and mitochondria-ER contact induce increased gluconeogenesis and impaired insulin signalling in the liver and muscle [17]; and neuron-type specific ablation impacts on energy metabolism [39, 40]. All this evidence points to Mitofusin 2 as a key regulator of insulin signalling [41]

Among the CMT causative genes, two of them are clearly involved in energy metabolism, *hexokinase-1* and *PDK3* [42, 43]. Most interestingly, the disease mechanism in *PDK3* mutation has been shown to be a hyperactivation of the PDK3 protein, which results in down-regulation of PDC [44]. This observation supports our hypothesis that elevated levels of *PDK* are related to the neurodegeneration in KU and KD models. Moreover, a reduction of glycolytic enzymes, including PyrK, is also a hallmark of one of the murine models of *GDAP1* [11].

This new evidence indicates that metabolic dysfunction may contribute to the neuronal and muscular degeneration either cell-autonomously and/or systemically. In consequence, the genes and metabolites involved in energy metabolism are promising candidates for biomarkers to evaluate disease progression in these neuropathies. The *Drosophila* model we present here is useful to understand the pathophysiology of clinical *GDAP1* mutations, to perform further metabolic studies for biomarker discovery and to find new treatments for the CMT neuropathy.

3. MATERIALS AND METHODS

3.1. *Drosophila* husbandry and genetics

OregonR and *Act5C-Gal4* stocks were obtained from the Bloomington *Drosophila* Stock Center. *UAS-Dcr2, UAS-Gdap1* and *UAS-Gdap1*^{RNAi} were described previously [13]. Flies were maintained on standard cornmeal medium at 25°C. The experimental genotypes were obtained by crossing *Act5C-Gal4* flies to *OregonR* (control), *UAS-Gdap1* (KU) and *UAS-Gdap1*^{RNAi}*, UAS-Dcr2* (KD).

3.2. Fitness, geotaxis and weight.

For the survival test, flies were cultured at 25°C, scored every 2-3 days and transferred to a new vial. This assay was done in triplicate for each genotype and at least 120 flies were counted per genotype. The negative geotaxis assay was conducted for 10-, 20- and 30-day old individuals. Flies were transferred to a tube without food and allowed to settle for 5 min. After knocking them down to the bottom of the vial, we scored the percentage of flies that reached the top of the vial (9 cm) in 10 seconds (Video S1). This assay was performed in quadruplicate for each genotype; at least 120 flies were used per genotype. To calculate individual weight, flies were anesthetized in groups of 15 individuals and weighed. This experiment was done in quintuplicate for each genotype.

3.3. Metabolite extraction.

Metabolite extraction was performed with the chloroform-methanol-water extraction procedure, widely applied for tissues and cells [45], which has been proven to be fast and

convenient and allows to quantify polar and non-polar metabolites. Briefly, flies were homogenized in groups of 15 individuals after adding methanol (240 µl), chloroform (120 µl) and water (48 µl) into plastic tubes on ice. Samples were vortexed and 120 µl of chloroform and 120 µl water were added, then vortexed again. Samples were kept 15 min on ice and then centrifuged at 4°C for 15 min, 10.000xg. At this point, two phases were obtained: an aqueous phase at the top and a chloroform phase at the bottom. The two phases were separated in different tubes, the aqueous phase was lyophilized and the chloroform of the organic phase was evaporated under vacuum. Samples were stored at -80°C.

3.4. NMR sample preparation.

Aqueous extracts were resuspended in 550 µl of NMR buffer (100 mM phosphate, in D_2O, pH 7.4, 0.1 mM 3-(trimethylsilyl)-2,2',3,3'-tetradeuteropropionic acid (TSP)). Samples were vortexed, centrifuged at 12.000xg for 5 min and the supernatant transferred to a 5 mm NMR tube. The organic extract was resuspended in 600 µl of deuterated chloroform with 0.03% v/v Tetramethylsilane (TMS) and centrifuged at 13.000xg for 1 min. 550 µl of the solution were transferred to an NMR tube, and the tube was sealed. Samples were stored at 4°C and measured the same day.

For intact fly samples [23, 46], flies were anesthetized and introduced in a 50-µl HRMAS rotor. At the top of the rotor, separated by parafilm, 50 µl of D2O was placed. HRMAS samples were measured immediately after preparation.

3.5. NMR spectroscopy.

NMR spectra of the extracts were recorded at 27ºC on a Bruker AVI-600 using a 5-mm TCI cryoprobe. The spectra of intact flies were recorded on a Bruker AVII-500 using a 5-mm

HRMAS probe with spinning at 2000 Hz. One-dimensional ^{1}H-NMR noesy spectra were acquired with 256 free induction decays (FIDs) for the aqueous extracts and 64 FIDs for chloroform extracts and intact flies. 64k data points were digitalized over a spectral width of 30 ppm for extract spectra and 20 ppm for HRMAS spectra. A 3 s relaxation delay was included between FIDs and water presaturation was applied for aqueous samples. The FID values were multiplied by an exponential function with a 0.5 Hz line broadening factor for extracts and 1 Hz for intact cells. Total Correlation Spectroscopy (TOCSY) and multiplicity Heteronuclear Single Quantum Correlation (HSQC) were performed for representative samples of the aqueous phase and the organic phase of each condition for signal assignment. For each of these experiments, 256-512 t1 increments were used and 32-96 transients were collected. The relaxation delays were set to 1.5 s and the experiments were acquired in the phase-sensitive mode. For extracts, TOCSY spectra were recorded using a standard MLEV-17 pulse sequence with mixing times (spin-lock) of 65 ms. For the extracts, the TOCSY spectra were recorded using a standard MLEV-17 pulse sequence with mixing times (spin-lock) of 65 µs. For the intact cells, the adiabatic TOCSY experiments [47] were acquired with tangential frequency modulation using an adiabatic pulse length of 285 µs and a mixing time of 60 ms.

3.6. Metabolite assignment and quantification.

Metabolite identification and assignment was performed with the help of databases (Amix, HMBD [48] and Biological Magnetic Resonance Data Bank), literature values and information from 2D NMR experiments. For specific metabolites the assignment was confirmed by spiking experiments, consisting in the addition of the compound to a previously measured extract sample and the subsequent evaluation of the consistency between the newly appearing signals with the proposed assignment. For metabolite quantification, spectra were

automatically integrated at selected regions with MestreNova. For a better comparison between extract samples, integration values were normalized to total intensity to minimize the variability generated by the extraction procedure. In the case of the intact fly samples, the Eretic, an artificial signal that was previously calibrated with a reference sample [49], was used for metabolite quantification.

3.7. Multivariate analysis.

Multivariate data analysis was performed with SIMCAP 12.0 (Umetrics, Sweden) with the normalized integral values of polar metabolites. Integral tables were pareto scaled (each value is divided by the square root of the standard deviation of each variable) for an easier interpretation of the data and to take into account small signals. Additionally, mean centering was applied to improve the interpretability of the model. To build discriminant models, orthogonal projection on latent structure-discriminant analysis (OPLS-DA) [50] analysis was performed. OPLS-DA separates predictive variation (between classes) from non-predictive (within classes) variation in a single component, thus, clear separations in the score plots are obtained. Furthermore, the analysis of S-plots [51] (representation of the magnitude of the variables modelled by co-variation versus the reliability of the modelled correlation) allowed to define the metabolites that were essential for discrimination. To assess the quality of each model, the parameters R2X(cum) (variance of X taken into account by the model), RY(cum) (variance of Y that is predicted) and Q2(cum) (goodness of prediction) were evaluated. A Q2(cum) value ≥ 0.5 was considered indicative for a good model. Furthermore, the OPLS-DA models were validated by performing the permutation test [52] 20 times with equivalent PLS-models. The coefficients R2 and Q2 generated from the permutation test were compared to the R2 and Q2 value of the real model. If intercept R2 and Q2 values from the permutation

test were significantly smaller than Q2 of the real model, the model was regarded as predictable.

3.8. Mitochondrial ATP levels.

Mitochondria were isolated from groups of 30 flies for each genotype [13]. Fluorescence was normalized to the protein content determined by the Pierce BCA protein assay kit (Thermo Fisher Scientific, Inc.). Each sample was analyzed in triplicate.

3.9. Mitochondria-ER contacts.

We quantified total number of mitochondria in each rhabdomere and then we determined how many of them were in contact to the ER. With these figures we calculated the ratio of mitochondria in contact with the ER to the total number of mitochondria. 40 ommatidia, each one containing 7 neuronal cell bodies, were scored per genotype.

3.10. Quantitative RT-PCR.

RNA extraction was performed with Trizol Reagent in groups of 20 flies for each genotype. Reverse-transcription was made with qScript cDNA supermix (Quanta Biosciences, Gaithersburg, MD, USA). Quantitative real-time PCR was performed with 5' FAM-labeled probes of the Roche Universal Probe Library (Roche, Basel, Switzerland) in an Applied Biosystems 7900HT Fast Real-Time PCR system (Thermo Fisher Scientific, Inc.). PCR primer pairs and probes were determined using the Roche Universal Probe Library Assay Design Tool. Primer sequences and probes are indicated in the table below. Each sample was

analyzed in triplicate, and the expression was calculated according to the 22DDCt method. Expression levels were normalized relative to the expression of *Gapdh1* and *Rp49*.

3.11. Western blotting.

For Western blot analysis, 5 replicas were made for each genotype. For each individual sample, 25 fly heads were pooled. Extraction was carried out in RIPA buffer with protease and phosphatase inhibitors, samples were heated to 95°C for 5 min before loading. The samples were electrophoresed in 12% SDS – PAGE, and the separated proteins were transferred onto Nitrocellulose membrane (Whatman GmbH, Dassel, Germany). After transfer, membranes were blocked with BSA 5% in TBS-T. Primary antibodies were AKT (1:1000, Cell Signaling. #9272) and phosphor-AKT (Ser 473) (1:1000, Cell Signaling. #9271). The blots were washed three times with TBS-Tween and further incubated for 1 h with a secondary anti-rabbit antibody conjugated with horseradish peroxidase. The membrane was washed three times 5 min with TBS–Tween, Luminol ECL Western Blotting Detection Reagent (GE Healthcare, Little Chalfont, UK) was added onto the membrane, 1 ml/membrane, and chemiluminescence was detected in an ImageQuant LAS-4000 image reader (GE Healthcare). Results were then analyzed with the Image Gauge 4.0 software. Quantitation of the Akt proteins was carried out by comparing band intensity with an actin standard.

COMPETING INTERESTS

The authors declare that they do not have any competing interests.

FUNDING

This work was supported by a project grant from the Association Française contre les Myopathies [AFM 18540 to M.I.G]; a collaborative grant from International Rare Diseases Research consortium (IRDiRC) and Instituto de Salud Carlos III [IR11/TREAT-CMT to M.I.G. (partner 12) and F.V.P. (partner 8)]; funding from Instituto de Salud Carlos III through Biomedical Network Research Center for Rare Diseases and the INGENIO 2010 program to F.V.P.; and a project grant from the Spanish Government (Secretaría de Estado de Investigación, Desarollo e Innovación, Ministerio de Economía y Competitividad) [SAF2014-53977-R to A.P.]

REFERENCES.

[1] N. Barisic, K.G. Claeys, M. Sirotkovic-Skerlev, A. Lofgren, E. Nelis, P. De Jonghe, V. Timmerman, Charcot-Marie-Tooth disease: a clinico-genetic confrontation, Ann Hum Genet 72 (2008) 416-441.

[2] J.M. Schroder, Neuropathology of Charcot-Marie-Tooth and related disorders, Neuromolecular Med 8 (2006) 23-42.

[3] K. Itoh, K. Nakamura, M. Iijima, H. Sesaki, Mitochondrial dynamics in neurodegeneration, Trends in cell biology 23 (2013) 64-71.

[4] A. Kasahara, L. Scorrano, Mitochondria: from cell death executioners to regulators of cell differentiation, Trends Cell Biol 24 (2014) 761-770.

[5] R.V. Baxter, K. Ben Othmane, J.M. Rochelle, J.E. Stajich, C. Hulette, S. Dew-Knight, F. Hentati, M. Ben Hamida, S. Bel, J.E. Stenger, J.R. Gilbert, M.A. Pericak-Vance, J.M. Vance, Ganglioside-induced differentiation-associated protein-1 is mutant in Charcot-Marie-Tooth disease type 4A/8q21, Nat Genet 30 (2002) 21-22.

[6] A. Cuesta, L. Pedrola, T. Sevilla, J. Garcia-Planells, M.J. Chumillas, F. Mayordomo, E. LeGuern, I. Marin, J.J. Vilchez, F. Palau, The gene encoding ganglioside-induced differentiation-associated protein 1 is mutated in axonal Charcot-Marie-Tooth type 4A disease, Nat Genet 30 (2002) 22-25.

[7] A. Niemann, M. Ruegg, V. La Padula, A. Schenone, U. Suter, Ganglioside-induced differentiation associated protein 1 is a regulator of the mitochondrial network: new implications for Charcot-Marie-Tooth disease, J Cell Biol 170 (2005) 1067-1078.

[8] L. Pedrola, A. Espert, X. Wu, R. Claramunt, M.E. Shy, F. Palau, GDAP1, the protein causing Charcot-Marie-Tooth disease type 4A, is expressed in neurons and is associated with mitochondria, Hum Mol Genet 14 (2005) 1087-1094.

[9] N. Huber, S. Guimaraes, M. Schrader, U. Suter, A. Niemann, Charcot-Marie-Tooth disease-associated mutants of GDAP1 dissociate its roles in peroxisomal and mitochondrial fission, EMBO Rep 14 (2013) 545-552.

[10] D. Pla-Martin, C.B. Rueda, A. Estela, M. Sanchez-Piris, P. Gonzalez-Sanchez, J. Traba, S. de la Fuente, L. Scorrano, J. Renau-Piqueras, J. Alvarez, J. Satrustegui, F. Palau, Silencing of the Charcot-Marie-Tooth disease-associated gene GDAP1 induces abnormal mitochondrial distribution and affects Ca2+ homeostasis by reducing store-operated Ca2+ entry, Neurobiol Dis 55 (2013) 140-151.

[11] M. Barneo-Munoz, P. Juarez, A. Civera-Tregon, L. Yndriago, D. Pla-Martin, J. Zenker, C. Cuevas-Martin, A. Estela, M. Sanchez-Arago, J. Forteza-Vila, J.M. Cuezva, R. Chrast, F. Palau, Lack of GDAP1 induces neuronal calcium and mitochondrial defects in a knockout mouse model of charcot-marie-tooth neuropathy, PLoS Genet 11 (2015) e1005115.

[12] A. Niemann, N. Huber, K.M. Wagner, C. Somandin, M. Horn, F. Lebrun-Julien, B. Angst, J.A. Pereira, H. Halfter, H. Welzl, M.L. Feltri, L. Wrabetz, P. Young, C. Wessig, K.V. Toyka, U. Suter, The Gdap1 knockout mouse mechanistically links redox control to Charcot-Marie-Tooth disease, Brain 137 (2014) 668-682.

[13] V. Lopez Del Amo, M. Seco-Cervera, J.L. Garcia-Gimenez, A.J. Whitworth, F.V. Pallardo, M.I. Galindo, Mitochondrial defects and neuromuscular degeneration caused by altered expression of Drosophila Gdap1: implications for the Charcot-Marie-Tooth neuropathy, Hum Mol Genet 24 (2015) 21-36.

[14] F. Burte, V. Carelli, P.F. Chinnery, P. Yu-Wai-Man, Disturbed mitochondrial dynamics and neurodegenerative disorders, Nat Rev Neurol 11 (2015) 11-24.

[15] M. Roy, P.H. Reddy, M. Iijima, H. Sesaki, Mitochondrial division and fusion in metabolism, Current opinion in cell biology 33 (2015) 111-118.

[16] A. Mourier, E. Motori, T. Brandt, M. Lagouge, I. Atanassov, A. Galinier, G. Rappl, S. Brodesser, K. Hultenby, C. Dieterich, N.G. Larsson, Mitofusin 2 is required to maintain mitochondrial coenzyme Q levels, J Cell Biol 208 (2015) 429-442.

[17] D. Sebastian, M.I. Hernandez-Alvarez, J. Segales, E. Sorianello, J.P. Munoz, D. Sala, A. Waget, M. Liesa, J.C. Paz, P. Gopalacharyulu, M. Oresic, S. Pich, R. Burcelin, M. Palacin, A. Zorzano, Mitofusin 2 (Mfn2) links mitochondrial and endoplasmic reticulum function with insulin signaling and is essential for normal glucose homeostasis, Proc Natl Acad Sci U S A 109 (2012) 5523-5528.

[18] S. Ekins, N.K. Litterman, R.J. Arnold, R.W. Burgess, J.S. Freundlich, S.J. Gray, J.J. Higgins, B. Langley, D.E. Willis, L. Notterpek, D. Pleasure, M.W. Sereda, A. Moore, A brief review of recent Charcot-Marie-Tooth research and priorities, F1000Res 4 (2015) 53.

[19] A.H. Brand, N. Perrimon, Targeted gene expression as a means of altering cell fates and generating dominant phenotypes, Development 118 (1993) 401-415.

[20] A. Walter, U. Korth, M. Hilgert, J. Hartmann, O. Weichel, K. Fassbender, A. Schmitt, J. Klein, Glycerophosphocholine is elevated in cerebrospinal fluid of Alzheimer patients, Neurobiol Aging 25 (2004) 1299-1303.

[21] S.R. Kimball, L.S. Jefferson, Signaling pathways and molecular mechanisms through which branched-chain amino acids mediate translational control of protein synthesis, J Nutr 136 (2006) 227S-231S.

[22] J. Ilzecka, Z. Stelmasiak, J. Solski, S. Wawrzycki, M. Szpetnar, Plasma amino acids concentration in amyotrophic lateral sclerosis patients, Amino Acids 25 (2003) 69-73.

[23] V. Sarou-Kanian, N. Joudiou, F. Louat, M. Yon, F. Szeremeta, S. Meme, D. Massiot, M. Decoville, F. Fayon, J.C. Beloeil, Metabolite localization in living drosophila using High Resolution Magic Angle Spinning NMR, Scientific reports 5 (2015) 9872.

[24] M.S. Patel, L.G. Korotchkina, Regulation of the pyruvate dehydrogenase complex, Biochem Soc Trans 34 (2006) 217-222.

[25] J.Y. Jeong, N.H. Jeoung, K.G. Park, I.K. Lee, Transcriptional regulation of pyruvate dehydrogenase kinase, Diabetes Metab J 36 (2012) 328-335.

[26] L.P. Musselman, J.L. Fink, P.V. Ramachandran, B.W. Patterson, A.L. Okunade, E. Maier, M.R. Brent, J. Turk, T.J. Baranski, Role of fat body lipogenesis in protection against the effects of caloric overload in Drosophila, J Biol Chem 288 (2013) 8028-8042.

[27] K.N. Bharucha, P. Tarr, S.L. Zipursky, A glucagon-like endocrine pathway in Drosophila modulates both lipid and carbohydrate homeostasis, The Journal of experimental biology 211 (2008) 3103-3110.

[28] D.N. Gross, A.P. van den Heuvel, M.J. Birnbaum, The role of FoxO in the regulation of metabolism, Oncogene 27 (2008) 2320-2336.

[29] A.P. Arruda, B.M. Pers, G. Parlakgul, E. Guney, K. Inouye, G.S. Hotamisligil, Chronic enrichment of hepatic endoplasmic reticulum-mitochondria contact leads to mitochondrial dysfunction in obesity, Nature medicine 20 (2014) 1427-1435.

[30] E. Tubbs, P. Theurey, G. Vial, N. Bendridi, A. Bravard, M.A. Chauvin, J. Ji-Cao, F. Zoulim, B. Bartosch, M. Ovize, H. Vidal, J. Rieusset, Mitochondria-associated endoplasmic reticulum membrane (MAM) integrity is required for insulin signaling and is implicated in hepatic insulin resistance, Diabetes 63 (2014) 3279-3294.

[31] E.J. Rulifson, S.K. Kim, R. Nusse, Ablation of insulin-producing neurons in flies: growth and diabetic phenotypes, Science 296 (2002) 1118-1120.

[32] O. Puig, M.T. Marr, M.L. Ruhf, R. Tjian, Control of cell number by Drosophila FOXO: downstream and feedback regulation of the insulin receptor pathway, Genes & development 17 (2003) 2006-2020.

[33] A. Niemann, K.M. Wagner, M. Ruegg, U. Suter, GDAP1 mutations differ in their effects on mitochondrial dynamics and apoptosis depending on the mode of inheritance, Neurobiol Dis 36 (2009) 509-520.

[34] M. Zimon, J. Baets, G.M. Fabrizi, E. Jaakkola, D. Kabzinska, J. Pilch, A.B. Schindler, D.R. Cornblath, K.H. Fischbeck, M. Auer-Grumbach, C. Guelly, N. Huber, E. De Vriendt, V. Timmerman, U. Suter, I. Hausmanowa-Petrusewicz, A. Niemann, A. Kochanski, P. De Jonghe,

A. Jordanova, Dominant GDAP1 mutations cause predominantly mild CMT phenotypes, Neurology 77 (2011) 540-548.
[35] L. Palamiuc, A. Schlagowski, S.T. Ngo, A. Vernay, S. Dirrig-Grosch, A. Henriques, A.L. Boutillier, J. Zoll, A. Echaniz-Laguna, J.P. Loeffler, F. Rene, A metabolic switch toward lipid use in glycolytic muscle is an early pathologic event in a mouse model of amyotrophic lateral sclerosis, EMBO Mol Med 7 (2015) 526-546.
[36] S. Rosales-Corral, D.X. Tan, L. Manchester, R.J. Reiter, Diabetes and Alzheimer disease, two overlapping pathologies with the same background: oxidative stress, Oxid Med Cell Longev 2015 (2015) 985845.
[37] M. Cnop, H. Mulder, M. Igoillo-Esteve, Diabetes in Friedreich ataxia, J Neurochem 126 Suppl 1 (2013) 94-102.
[38] M.K. Jha, I.K. Lee, K. Suk, Metabolic reprogramming by the pyruvate dehydrogenase kinase-lactic acid axis: Linking metabolism and diverse neuropathophysiologies, Neurosci Biobehav Rev 68 (2016) 1-19.
[39] M.O. Dietrich, Z.W. Liu, T.L. Horvath, Mitochondrial dynamics controlled by mitofusins regulate Agrp neuronal activity and diet-induced obesity, Cell 155 (2013) 188-199.
[40] M. Schneeberger, M.O. Dietrich, D. Sebastian, M. Imbernon, C. Castano, A. Garcia, Y. Esteban, A. Gonzalez-Franquesa, I.C. Rodriguez, A. Bortolozzi, P.M. Garcia-Roves, R. Gomis, R. Nogueiras, T.L. Horvath, A. Zorzano, M. Claret, Mitofusin 2 in POMC neurons connects ER stress with leptin resistance and energy imbalance, Cell 155 (2013) 172-187.
[41] A. Zorzano, M.I. Hernandez-Alvarez, D. Sebastian, J.P. Munoz, Mitofusin 2 as a driver that controls energy metabolism and insulin signaling, Antioxid Redox Signal 22 (2015) 1020-1031.
[42] J. Hantke, D. Chandler, R. King, R.J. Wanders, D. Angelicheva, I. Tournev, E. McNamara, M. Kwa, V. Guergueltcheva, R. Kaneva, F. Baas, L. Kalaydjieva, A mutation in an alternative untranslated exon of hexokinase 1 associated with hereditary motor and sensory neuropathy -- Russe (HMSNR), Eur J Hum Genet 17 (2009) 1606-1614.
[43] M.L. Kennerson, E.M. Yiu, D.T. Chuang, A. Kidambi, S.C. Tso, C. Ly, R. Chaudhry, A.P. Drew, G. Rance, M.B. Delatycki, S. Zuchner, M.M. Ryan, G.A. Nicholson, A new locus for X-linked dominant Charcot-Marie-Tooth disease (CMTX6) is caused by mutations in the pyruvate dehydrogenase kinase isoenzyme 3 (PDK3) gene, Hum Mol Genet 22 (2013) 1404-1416.
[44] G. Perez-Siles, C. Ly, A. Grant, A.P. Drew, E.M. Yiu, M.M. Ryan, D.T. Chuang, S.C. Tso, G.A. Nicholson, M.L. Kennerson, Pathogenic mechanisms underlying X-linked Charcot-Marie-Tooth neuropathy (CMTX6) in patients with a pyruvate dehydrogenase kinase 3 mutation, Neurobiol Dis 94 (2016) 237-244.
[45] O. Beckonert, H.C. Keun, T.M. Ebbels, J. Bundy, E. Holmes, J.C. Lindon, J.K. Nicholson, Metabolic profiling, metabolomic and metabonomic procedures for NMR spectroscopy of urine, plasma, serum and tissue extracts, Nature protocols 2 (2007) 2692-2703.
[46] V. Righi, Y. Apidianakis, D. Mintzopoulos, L. Astrakas, L.G. Rahme, A.A. Tzika, In vivo high-resolution magic angle spinning magnetic resonance spectroscopy of Drosophila melanogaster at 14.1 T shows trauma in aging and in innate immune-deficiency is linked to reduced insulin signaling, International journal of molecular medicine 26 (2010) 175-184.
[47] W. Peti, C. Griesinger, W. Bermel, Adiabatic TOCSY for C,C and H,H J-transfer, Journal of biomolecular NMR 18 (2000) 199-205.
[48] D.S. Wishart, T. Jewison, A.C. Guo, M. Wilson, C. Knox, Y. Liu, Y. Djoumbou, R. Mandal, F. Aziat, E. Dong, S. Bouatra, I. Sinelnikov, D. Arndt, J. Xia, P. Liu, F. Yallou, T. Bjorndahl, R. Perez-Pineiro, R. Eisner, F. Allen, V. Neveu, R. Greiner, A. Scalbert, HMDB 3.0--The Human Metabolome Database in 2013, Nucleic acids research 41 (2013) D801-807.
[49] G. Nuzzo, C. Gallo, G. d'Ippolito, A. Cutignano, A. Sardo, A. Fontana, Composition and quantitation of microalgal lipids by ERETIC (1)H NMR method, Marine drugs 11 (2013) 3742-3753.

[50] M. Bylesjo, A. Sjodin, D. Eriksson, H. Antti, T. Moritz, S. Jansson, J. Trygg, MASQOT-GUI: spot quality assessment for the two-channel microarray platform, Bioinformatics 22 (2006) 2554-2555.
[51] S. Wiklund, E. Johansson, L. Sjostrom, E.J. Mellerowicz, U. Edlund, J.P. Shockcor, J. Gottfries, T. Moritz, J. Trygg, Visualization of GC/TOF-MS-based metabolomics data for identification of biochemically interesting compounds using OPLS class models, Analytical chemistry 80 (2008) 115-122.
[52] F. Pesarin, Multivariate permutation tests: with applications in biostatistics, John Wiley and Sons, Chichester, United Kingdom, 2001.